https://doi.org/10.5194/hess-2022-66
Preprint. Discussion started: 23 February 2022

Hydrology and Earth System Sciences
Open Access
Discussions

Statistical characteristics of raindrop size distribution during rainy seasons in Complicated Mountain Terrain

Wenqian Mao[1,2,3], Wenyu Zhang[1,2,3*], Menggang Kou[1]

1. School of Geoscience and Technology, Zhengzhou University, Zhengzhou, 450001, China
2. Key Laboratory for Cloud Physics, Chinese Academy of Meteorological Sciences, Beijing 100081, China
3. College of Atmospheric Sciences, Lanzhou University, Lanzhou, 730000, China

Correspondence to: Wenyu Zhang (zhangwy@zzu.edu.cn)

Abstract: In order to understand the differences of raindrop size distribution (DSD) in complex mountainous terrain, the characteristics of DSD were analyzed by using the six-months observation data at the southern slopes, northern slopes and inside in Qilian Mountains. For all rainfall events, the number concentration of small and large raindrops on the inside and south slope are greater than that on the north slope, but midsize raindrops are less. The DSD spectrum of inside mountains are more variable and significantly differ from the north slopes. The differences in normalized intercept parameters of DSD for stratiform and convective rainfall are 8.3% and 10.4%, respectively, and mass-weighted diameters are 10.0% and 23.4%, respectively, which the standard deviation of DSD parameters on inside sites are larger. The differences in coefficient and exponent of Z-R relationship are 2.5% and 10.7%, respectively, with an increasing value of coefficient from the south slope to the north slope in stratiform rainfall but opposite to convective rainfall. In addition, the DSD characteristics and Z-R relationships are more similar at the ipsilateral sites and have smaller differences between the south slope and inside mountains.

Keywords: *Raindrop size distribution; Complicated mountain terrain;* characteristic difference

https://doi.org/10.5194/hess-2022-66
Preprint. Discussion started: 23 February 2022

1 Introduction

Raindrop size distribution (DSD), the number of raindrops per drop size per unit volume, is an important parameter to statistically describe the microstructure of precipitation（Bringi et al., 2003; Ma et al., 2019a）. The measurement of DSD can provide some fundamental information such as raindrop size (D), liquid water content (W), rain rate (R), radar reflectivity factor (Z) and so on, which has an essential contribution to improving quantitative precipitation estimates (QPE) using weather radar and satellite observations (Adirosi et al., 2018; Jash et al., 2019). The parameterization of DSD can obtain the distribution model parameters of DSD in different rain types, which is significant to advance microphysics parameterization in numerical weather prediction (NWP) models (Wainwright et al., 2014; McFarquhar et al., 2015; Zhao et al., 2019). In addition, understanding the DSD is crucial in many application fields concerning hydrology, agriculture, soil erosion and microwave communication (Rincon et al., 2002; Smith et al., 2009; Angulo-Martínez et al., 2015; Lim et al., 2015; Yang et al., 2016).

Numerous studies have been carried out the statistical characteristics of DSD in different regions (Campos et al., 2006; Seela et al., 2017; Dolan et al., 2018; Protat et al., 2019; Loh et al., 2019; Jash et al., 2019). It is shown that the number concentration and size of raindrops increase with rain rate and so DSD becomes higher and wider. The characteristics in different rain types display that the mass-weighted mean diameter (i.e., D_m) and normalized intercept parameter (i.e., N_w) of convective rainfall (CR) are larger than those of stratiform rainfall. (SR). Furthermore, these studies also reveal that there are more differences in characteristics of DSD. Dolan et al. (2018) divided global DSD characteristics into 6 types by using 12 datasets across three latitudes and found centralized regions and DSD parameters of 6 types varied in location. The average number of raindrops in central Korea were usually more numerous than that in southeast under three rainfall systems, especially drops on 0.31-0.81mm diameter range (Loh et al., 2019). According to the DSD results from Tibetan Plateau (TP), it showed the eastern regions had higher number concentration of raindrops on 0.437-1.625mm diameters and more variation on different diameters than that in central regions (Wang et al., 2020). Compared to eastern China and northern China, the DSD in southern China demonstrated a higher number concentration of relatively small-sized drops, respectively (Zhang et al., 2019). The comparison of Z-R relationship (defined as $Z=AR^b$) indicated that coefficient decreased with increasing R in southern TP, which is opposite in south China (Wu et al., 2017). For the DSD parameters of SR and CR, there are various changes between the lower reaches and middle reaches of Yangtze River (Fu et al., 2020).

As reported in above studies, DSD characteristics significantly vary with factors such as geographical location, climatic region and rain types. Pu et al. (2020) analyzed the DSD characteristics of five sites in Najing city and found N_w of DSD was largest at site near industrial areas but D_m of DSD was largest at site near city's centre. In other words, even at urban scale, there are still differences to microphysical characteristics reflected by the DSD which is due to the influence of the surrounding environment. Then how do the characteristics of DSD vary from location for the complicated mountain terrain? Rao et al. (2006) suggested that the obvious variation in DSD with altitude were related to evaporation and breakup by comparing the DSD parameters at different altitudes. Geoffroy et al. (2014) concluded that the total concentration of raindrops decreased while the average drop size increased as decreasing altitude, which used aircraft observations. Then how large would be the differences in DSD at different altitudes in mountainous region? And then how significant would be the effects of these differences?

Qilian mountains, a series of marginal mountains in the northeastern part of TP, are the vitally important ecological protection barrier in northwest arid areas, which block the connection of deserts and wilderness in the northwest (shown as Figure 1). The mountains form several inland rivers that are important water source for the northwest arid areas and have made a considerable contribution to regional economic development (Gou et al., 2005; Tian et al., 2014; Qin et al., 2016). In this paper, we choose Qilian mountains as the research object and select 6 sites with different backgrounds representing the southern slopes, northern slopes and inside of Qilian mountains. To thoroughly investigate the discrepancies in the complicated mountain terrain, the DSD characteristics and Z-R relationships are comprehensively analyzed according to different rain types based on continuous disdrometer observations in rainy season. The primary goal is to obtain the finer precipitation of Qilian mountains and improve the accuracy of QPE, which would be as research foundation for developing cloud water resources in mountainous areas.

2 Data and method

2.1 Sites and instruments

The eastern and middle sections of the Qilian Mountains were chosen as the main study area, taking into account that several important inland rivers originating from these areas of Qilian Mountains (Li et al., 2019). Six disdrometers were deployed on the southern slopes, northern slopes and inside (close to the ridge) of Qilian mountains, with three sites in the eastern section which called Taola (TL), Huangchengshuiguan (HS), and Liuba (LB) from south to north, and with another three sites in the middle section which called Daladong (DLD), Boligou (BLG), Shandan (SD) from south to north. The background of Qilian Mountains is shown on the satellite map, and the six sites are marked on the topographical map, as Figure 1. The distances between six sites are listed in Table 1. The sites on the south, north and inside are basically parallel to the trend of the mountain, and the sections formed by the sites in the east and middle are basically perpendicular to the trend of the mountain. Through the historical weather review and rain gauge observation results, the rainy season at the six sites is concentrated in May to October, with more precipitation in July, August and September.

https://doi.org/10.5194/hess-2022-66
Preprint. Discussion started: 23 February 2022

Hydrology and Earth System Sciences
Discussions

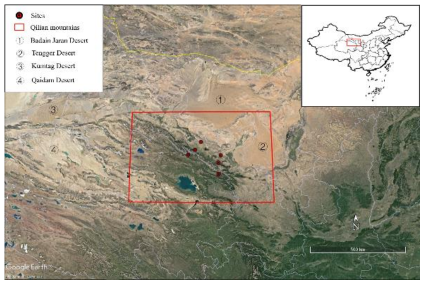

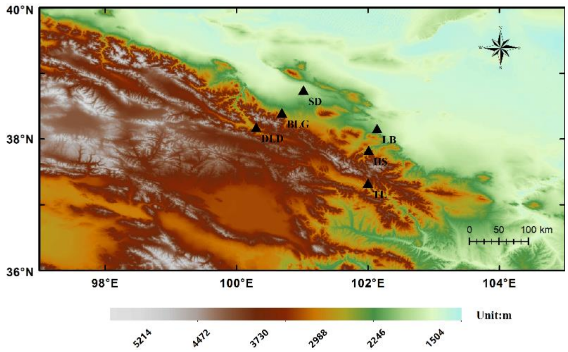

Fig.1 The Geographical overview of Qian mountains and the disdrometer sites; the circles or triangles represent the location of the sites. The map above is from Google Earth © Google Earth

Table 1 Location between every two sites (latitude, longitude, sea level height and distance information).

Six sites distance (km)	LB	HS	TL	SD	BLG	DLD
LB (38.16˚N, 102.14˚E, 1926m)	-	39.6	94.3	116.0	129.6	161.1
HS (37.83˚N, 102.01˚E, 2342m)	-	-	55.6	135.1	132.8	154.9
TL (37.33˚N, 102.00˚E, 2910m)	-	-	-	182.4	167.3	177.0
SD (38.80˚N, 101.08˚E, 1765m)	-	-	-	-	54.2	96.8
BLG (38.4˚N, 100.69˚E, 2455m)	-	-	-	-	-	43.3
DLD (38.18˚N, 100.3˚E, 2957m)	-	-	-	-	-	-

This experiment used an optical, laser-based device to measure DSD, called DSG4 disdrometer, which met the assessment of Functional Specification Requirements For Disdrometer issued by the China Meteorological Administration. The disdrometer has the HSC-OTT Parsivel2 sensor as observation part manufactured by OTT Messtechnik (Germany) and Huatron (China). When raindrops pass through the horizontal flat laser beam generated by the transmitting part of the instrument, it causes the signal attenuation in the laser observation area. The raindrop size is determined by the degree of signal attenuation and the falling speed is recorded by the transit time. The sampling time is 60s and the velocity and drop sizes are divided into 32 non- equally spaced bins, varying from 0.05 to 20.8 m s−1 for velocity and 0.062 to 24.5 mm for drop diameter.

https://doi.org/10.5194/hess-2022-66
Preprint. Discussion started: 23 February 2022

2.2 Quality control of the data

It is necessary to carry out quality control on the data due to potential instrument error. Every minute of DSD has been carefully processed, which collected by the six DSG4 disdrometers from May to October 2020. The following criteria have been employed in choosing data for analysis (Zhang et al., 2019). (1) The first two size bins were ignored because of low signal-to-noise ratio; (2) samples with 1-min total number of raindrops less than 10 or rain rate at moment of discontinuous observation less than 0.1 mmh^{-1} were regarded as noise; (3) raindrops at the diameter of more than 8 mm were eliminated; (4) raindrop with a falling terminal velocity V(D_i) that deviates from the empirical terminal velocity Vemp(D_i) more than 40% were removed (Kruger and Krajewski, 2002); and (5) samples with less than 5 bins after the correction of falling terminal velocity were deleted because its DSD can't be determined with too few bins.

$$\left|V(D_i) - V_{emp}(D_i)\right| < 0.4V_{emp}(D_i) \tag{1}$$

where $V_{emp}(D_i) = 9.65 - 10.3\exp(-0.6D_i)$ (D_i is the mean volume-equivalent diameter of the ith size category), as derived from the formula given in Atlas et al. (1973).

2.3 Integral parameters of rainfall

The basic observations obtained by disdrometer is counts of raindrops at each diameter and velocity. And the diameters given by disdrometer are the mid value of two adjacent bins, which we take the diameters as the corresponding endpoint bin values. The velocities are weighted average velocity class over the corresponding disdrometer. The raindrop number concentration N(D_i) (m^{-3}mm^{-1}) in the ith size bin per unit volume per unit size interval for diameter is calculated the following equation:

$$N(D_i) = \sum_{i.j=1}^{32} \frac{n_{i,j}}{A \cdot \Delta t \cdot V_j \cdot \Delta D_i} \tag{2}$$

Where $n_{i,j}$ is the counts of raindrops measured by disdrometer within the size bin i and velocity bin j during sampling time Δt; A and Δt are the sampling area (0.0054 m^2) and sampling time (60 s), respectively; V_j (m s^{-1}) is the mid-value falling speed for velocity bin j; ΔD_i is the diameter spread for the ith diameter bin.

Some integral rainfall parameters, such as total number concentration N_t (m^{-3}), rain rate R (mm h^{-1}), radar reflectivity factor Z (mm^6 m^{-3}) and liquid water content W (g cm^{-3}), can be derived by the following equation:

$$N_t = \sum_{i=1}^{32} N(D_i)\Delta D \tag{3}$$

$$R = \frac{6\pi}{10^4 \rho_w} \sum_{i=1}^{32} V(D_i)\, D_i^3 N(D_i)\Delta D_j \tag{4}$$

$$Z = \sum_{i=1}^{32} N(D_i) D_i^6 \Delta D_i \tag{5}$$

https://doi.org/10.5194/hess-2022-66
Preprint. Discussion started: 23 February 2022

$$W = \frac{\pi \rho_w}{6 \times 10^3} \sum_{i=1}^{32} D_i^3 N(D_i) \Delta D_i \tag{6}$$

where ρ_w is water density (1.0 gcm^{-3}); $V(D_i)$ is the falling speed measurements from disdrometer. In this study, when calculating rain rate we use $V_{emp}(D_i)$ to replace $V(D_i)$ because of measurement error, particularly at larger bins and faster falling speeds.

The DSD characteristics can be described by three-parameter gamma distribution in following form. And it has better capability than M-P distribution to describe the broader variation of DSD fluctuations, which has been proven to be well fitted the main part of spectra and reduce the fitting error on small and large scale.

$$N(D) = N_0 D^{\mu} \exp(-\Lambda D) \tag{7}$$

where N(D) is the raindrop number concentration; D is the raindrop bins with unit mm; N_0, μ and Λ are intercept, shape and slope parameter from three parameters of gamma model which can be derived from gamma moments or least square method, respectively. When μ=0, it degenerates into M-P DSD model.

Although, three-parameter gamma distribution is commonly accepted model, the normalized gamma model has been widely adopted with its independent parameters and clear physical meaning as follows:

$$N(D) = \frac{3}{128} N_w \left[\frac{(4+\mu)^{(4+\mu)}}{\Gamma(4+\mu)}\right] \left(\frac{D}{D_m}\right)^{\mu} \exp\left(\frac{-(4+\mu)D}{D_m}\right) \tag{8}$$

Where μ is the shape parameter in dimensionless; D_m (mm) is the mass-weighted mean diameter and N_w (m^{-3} mm^{-1}) is the normalized intercept parameter computed from D_m. The form is as follows:

$$D_m = \frac{\sum_{i=1}^{32} N(D_i) D_i^4 \Delta D_i}{\sum_{i=1}^{32} N(D_i) D_i^3 \Delta D_i} \tag{9}$$

$$N_w = \frac{4^4}{\pi \rho_w} \left(\frac{10^3 W}{D_m^4}\right) \tag{10}$$

3 DSD parameter characteristics

3.1 Characteristics of DSD

The number of 1 min DSD spectra from six sites have been selected after data quality control covering the rainy season (May-October) in the Qilian Mountains region in 2020, which are accounted for 87.9%, 85.8%, 84.5%, 91.2%, 80.6%, 86.5% of the total number of samples to LB, HS, TL, SD, BLG, DLD, respectively. Figure 2a shows the mean DSDs for the six districts in Qilian mountains. The maximum concentration of raindrops is around on 0.562mm diameter and the maximum number concentration values of sites are BLG>TL>DLD>HS>SD>LB. As the increasing diameter, the number concentration values decrease and the concentration values are LB>SD>DLD>TL>BLG>HS at around 2 mm diameter. When the diameter is larger than 4 mm, the concentration of TL, BLG and HS are relatively high. In this study, it is roughly divided into small raindrops (less than 1 mm in diameter), midsize raindrops

https://doi.org/10.5194/hess-2022-66
Preprint. Discussion started: 23 February 2022

(1-3 mm) and large raindrops (greater than 3 mm) to easily describe the difference of DSDs (Ma et al., 2019b; Pu et al., 2020). To highlight the DSD differences caused by background environment, Figure 2b shows the mean DSDs normalized with N_w and D_m results for sites. Compared with Figure 2a, the characteristics of the raindrops are more consistent across sizes, while the differences between the above sites are more pronounced, especially in the medium and large raindrops, which truly reflects the DSD differences caused by location variability. Combining the characteristics of the geographical environment of the six sites, we can analyze some differences in DSD characteristics in Qilian Mountains. For small raindrops, the number concentrations on the inside and southern slopes districts are greater than that on the northern slopes; for midsize raindrops, the number concentrations decrease sequentially on the northern slopes, southern slopes and inside districts; for large raindrops, the number concentrations on the inside districts are larger. In addition, the number concentrations of raindrops in the middle section of the mountainous area is slightly greater than that in the eastern section.

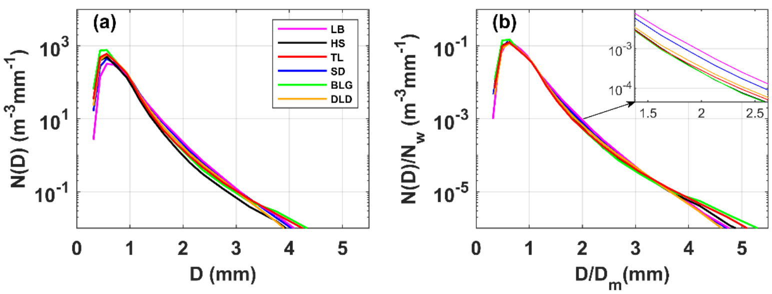

Fig.2 (a) Mean measured DSDs; (b) Normalized mean DSDs at six sites of Qilian mountains region in rainy season

3.2 Distribution of DSD parameters

In order to study the differences in DSDs, we selected 6 integral rainfall parameters for discussion, which are normalized intercept parameter (N_w), mass-weighted mean diameter (D_m), shape parameter (μ), total number concentration (N_t), rain rate (R) and radar reflectivity factor (Z). Figure 3 and Table 2 show the distribution and statistics of 6 DSD parameters (the distribution of each parameter is normalized using the uniform method). Averagely, Dm is more concentrated on smaller values at HS and BLG, which shows smaller mean values than TL and DLD, while significantly more values greater than 1mm at LB and SD; log10Nw is more centralized on larger values at TL and DLD, with relatively smaller values at LB and SD; the distribution patterns for μ and log10Nt are similar to those for log10Nw. The density curves of R and Z are similar, but there are differences at the 6 sites, which would be analyzed in detail in subsequent content. It is noteworthy that the frequency of samples with R around 0.6-1.0 mmh^{-1} is highest, and samples with R less than $1mmh^{-1}$ account for more than half of the total rainfall.

https://doi.org/10.5194/hess-2022-66
Preprint. Discussion started: 23 February 2022

Hydrology and Earth System Sciences
Open Access
Discussions

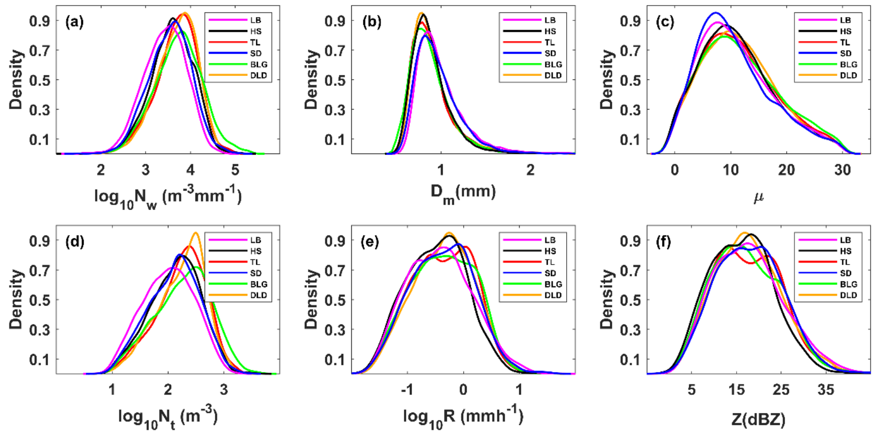

Fig.3 Probability density distribution of integral DSD parameters at six sites (LB, HS, TL, SD, BLG, DLD): (a) normalized intercept parameter log10Nw ($m^{-3}mm^{-1}$); (b) mass-weighted mean diameter Dm (mm); (c) shape parameter μ; (d) total number concentration $\log_{10}N_t$ (m^{-3}); (e) rain rate R (mmh^{-1}); (f) radar reflectivity factor Z (mm^6mm^{-3})

Table 2 Statistical of several integral DSD parameters for all observations at six sites (LB, HS, TL, SD, BLG, DLD).

Sites	$Log_{10}N_w$ ($m^{-3}mm^{-1}$)			D_m (mm)			μ			$Log_{10}N_t$ (m^{-3})			R (mmh^{-1})			Z dBZ		
	ME	SD	SK	ME	SD	SK	ME	SD	SK	ME	SD	SK	ME	SD	SK	ME	SD	SK
LB	3.43	0.47	-0.25	0.99	0.29	2.68	10.92	6.63	0.61	2.01	0.46	-0.07	0.94	1.90	0.23	17.79	7.82	0.44
HS	3.59	0.48	-0.29	0.89	0.25	3.35	11.12	6.64	0.53	2.13	0.45	-0.22	0.69	1.60	0.05	16.24	7.08	0.34
TL	3.69	0.48	-0.55	0.90	0.29	4.49	11.37	6.84	0.48	2.23	0.44	-0.43	0.89	1.48	-0.05	17.47	7.55	0.35
SD	3.54	0.48	-0.17	0.96	0.26	2.12	10.62	6.61	0.71	2.11	0.46	-0.17	0.97	2.01	0.06	17.95	7.47	0.28
BLG	3.72	0.54	-0.15	0.89	0.29	5.17	11.71	7.06	0.46	2.26	0.50	-0.25	0.94	2.13	-0.04	17.34	7.66	0.41
DLD	3.69	0.45	-0.50	0.90	0.25	2.66	11.52	6.66	0.43	2.24	0.43	-0.46	0.95	1.62	-0.01	17.70	7.43	0.37

Note: ME is mean; SD is standard deviation; SK is skewness.

3.3 Characteristics of DSD in different rain rate classes

To further understand the characteristics of DSDs at the six sites, the samples are divided into six classes according to the associated rain rate (R): C1, R<0.5; C2, 0.5≤R<2; C3, 2≤R<4; C4, 4≤R<6; C5, 6≤R<10; C6, R≥10mmh^{-1}. Such classification is based on two considerations: firstly, the number of observation samples in different rainfall rates roughly conformed to a normal distribution; and secondly, the mean maximum diameter interval of different rainfall rates gradually increases (Li et al., 2019). Of course, other studies about classification are referenced and the fact that the rain rate in this area is smaller than that in the southern China is taken into account (Ma et al., 2019b; Zeng et al., 2021). Figure 4 shows the mean DSDs at each rain rate class for six sites. Table 3 contains the number of samples and statistical values of the DSD

https://doi.org/10.5194/hess-2022-66
Preprint. Discussion started: 23 February 2022

Hydrology and Earth System Sciences
Open Access
Discussions

parameters for six classes. Obviously, with the rain rate class increasing, the number concentration of almost all raindrop sizes and the width of DSD shapes increase, thus the tail of DSD shape gradually moves towards a larger diameter, which are similar to the previous studies such as Ma et al. (2019b) and Pu et al. (2020). Taking a number concentration of 0.01 $m^{-3}mm^{-1}$, the mean maximum diameter of DSD in each class is in order: 2.3-2.5, 3.2-3.4, 3.9-4.5, 4.3-5.0, 5.0-5.6 and 6.0-7.0 mm (The sixth-class diameter range is not fully shown in the figure). In class C1, the number concentrations are relatively similar in different sites; starting from class C2, the differences of number concentration increase when the diameter is greater than 2mm for 6 sites; and the differences of number concentration are gradually reflected on each raindrop size bin as rain rate class increasing. Observingly, the DSDs of BLG, HS and TL have larger number concentrations in different rain rate class, and the DSD parameters and standard deviations (SD) are larger, especially for BLG.

Table 3 Statistical of several integral DSD parameters for six rain rate classes at 6 sites.

Class	Sites	Samples	$Log_{10}N_w$ ($m^{-3}mm^{-1}$)		D_m (mm)		μ		$Log_{10}N_t$ (m^{-3})		R (mmh^{-1})		Z dBZ	
			ME	SD	ME	SD	ME	SD	ME	SD	ME	SD	ME	SD
C1(<0.5 mm h^{-1})	LB	6520	3.25	0.41	0.88	0.18	12.36	7.09	1.74	0.34	0.20	0.13	12.68	4.52
	HS	10753	3.43	0.44	0.81	0.17	12.01	7.03	1.89	0.37	0.20	0.13	11.90	4.54
	TL	7858	3.52	0.44	0.79	0.16	12.91	7.12	1.96	0.37	0.20	0.13	11.78	4.16
	SD	5772	3.34	0.43	0.85	0.18	11.72	6.99	1.82	0.36	0.20	0.13	12.51	4.40
	BLG	10073	3.50	0.48	0.79	0.17	12.94	7.28	1.94	0.40	0.20	0.13	11.73	4.26
	DLD	6891	3.51	0.43	0.79	0.15	13.04	6.92	1.96	0.36	0.21	0.13	12.14	4.15
C2(0.5~2 mm h^{-1})	LB	3318	3.66	0.41	1.06	0.24	9.93	5.75	2.30	0.28	1.00	0.41	22.55	3.27
	HS	5700	3.82	0.39	0.97	0.21	10.21	5.88	2.44	0.26	0.96	0.37	21.67	3.09
	TL	5368	3.87	0.42	0.98	0.23	10.35	6.15	2.49	0.26	1.07	0.41	22.18	3.33
	SD	3778	3.73	0.41	1.03	0.23	9.94	6.14	2.36	0.28	1.02	0.40	22.40	3.15
	BLG	6411	3.97	0.47	0.94	0.25	11.24	6.72	2.56	0.30	1.07	0.43	21.69	3.69
	DLD	4778	3.88	0.37	0.95	0.20	10.91	6.02	2.47	0.24	1.01	0.40	21.60	3.19
C3(2~4 mm h^{-1})	LB	782	3.71	0.47	1.31	0.37	7.33	4.28	2.52	0.29	2.77	0.56	29.54	2.87
	HS	884	3.96	0.50	1.16	0.34	8.42	5.22	2.73	0.27	2.76	0.54	28.33	3.06
	TL	1232	4.00	0.47	1.13	0.33	8.70	5.93	2.75	0.23	2.68	0.53	28.07	3.16
	SD	812	3.89	0.44	1.19	0.27	8.57	5.53	2.63	0.26	2.71	0.53	28.41	2.68
	BLG	1865	4.05	0.49	1.11	0.30	8.62	5.75	2.81	0.25	2.70	0.53	27.99	3.29
	DLD	1111	3.91	0.44	1.18	0.29	7.81	5.45	2.70	0.23	2.74	0.54	28.73	3.09
C4(4~6 mm h^{-1})	LB	229	3.80	0.47	1.41	0.40	7.33	3.94	2.65	0.31	4.76	0.57	32.69	2.63
	HS	191	4.03	0.54	1.28	0.47	7.54	4.42	2.86	0.27	4.80	0.56	31.70	3.34
	TL	213	3.84	0.56	1.41	0.51	6.23	4.64	2.77	0.28	4.77	0.54	32.82	3.54
	SD	187	4.03	0.41	1.24	0.27	8.35	5.02	2.80	0.22	4.76	0.54	31.32	2.52
	BLG	321	3.99	0.66	1.33	0.53	7.97	6.10	2.93	0.27	4.78	0.54	32.44	4.40
	DLD	270	3.92	0.53	1.35	0.47	6.50	4.80	2.83	0.25	4.83	0.56	32.55	3.47
C5(6~10 mm h^{-1})	LB	167	3.81	0.46	1.55	0.44	6.46	3.38	2.72	0.27	7.66	1.22	35.74	2.85
	HS	49	3.69	0.74	1.70	0.68	6.89	4.82	2.75	0.38	7.42	1.09	36.14	4.29

	TL	103	3.57	0.62	1.78	0.66	5.20	4.62	2.71	0.32	7.32	1.02	37.03	3.76
	SD	128	3.96	0.39	1.42	0.35	7.10	3.96	2.82	0.21	7.68	1.17	34.76	2.42
	BLG	138	3.97	0.76	1.51	0.80	8.34	6.35	2.99	0.27	7.37	1.02	35.09	4.96
	DLD	122	3.90	0.46	1.46	0.34	6.13	4.20	2.86	0.26	7.29	1.11	35.32	2.88
C6(>10 mm h^{-1})	LB	87	3.85	0.44	1.73	0.53	5.08	3.05	2.87	0.32	14.81	7.57	39.58	3.57
	HS	42	3.60	0.65	2.19	0.92	6.74	5.27	3.00	0.28	21.69	9.91	42.93	6.11
	TL	40	3.16	0.69	2.69	1.19	4.34	5.20	2.74	0.32	18.25	9.69	44.70	5.41
	SD	59	3.66	0.29	2.04	0.46	3.30	2.48	2.91	0.16	21.07	8.34	42.85	4.10
	BLG	53	3.38	0.93	2.58	1.52	5.58	6.19	3.00	0.37	21.95	9.05	44.08	7.50
	DLD	58	3.82	0.47	1.80	0.46	6.64	4.12	2.84	0.28	16.58	7.21	40.13	3.53

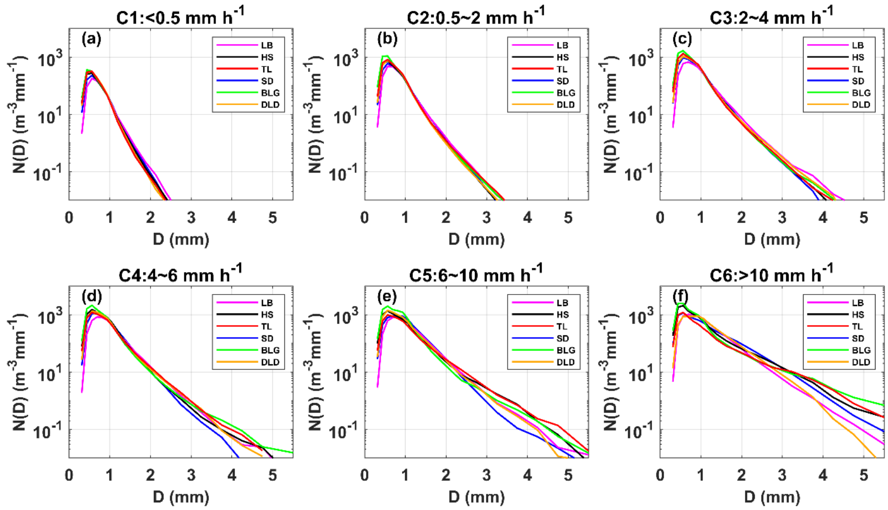

Fig.4 Distribution of mean measured DSD for different rain rate classes at 6 sites.

Fig. 5 shows box-whisker plots of the normalized intercept parameter $\log_{10}N_w$ and mass-weighted mean diameter D_m for 6 sites at each rain rate class. The middle line in the box indicates the median. The left and right lines in the box indicate the 25th and 75th. The left and right ends of whiskers indicate the most extreme data points between 5th and 95th, except outliers. The median of D_m gradually increases with a larger value range when the rain rate class increases, particularly for HS and BLG at class C5 and C6. The median of $\log_{10}N_w$ increases at class C1 to C3 and then tends to decrease at class C5 to C6, which the reduction is obvious at sites with a larger value range, such as HS and BLG. Ma et al. (2019b) also obtains similar conclusions about D_m and $\log_{10}N_w$. It is indicated that the increase of rain rate is mainly due to the growth in raindrop size. And the change of number concentration may be caused by the imbalance between the loss of number concentration at small raindrop size and the addition at large raindrop size, which implies in a sense that the relation of collision-coalescence and break-up of raindrops. It is worth noting that the microphysical processes are quite different among the sites, which are greatly influenced by the surrounding environment. Because HS and BLG are located on the inside mountains and close to ridge, thus their dynamics and thermodynamics as well underlying surface are different from other

https://doi.org/10.5194/hess-2022-66
Preprint. Discussion started: 23 February 2022

Hydrology and Earth System Sciences
Discussions

districts.

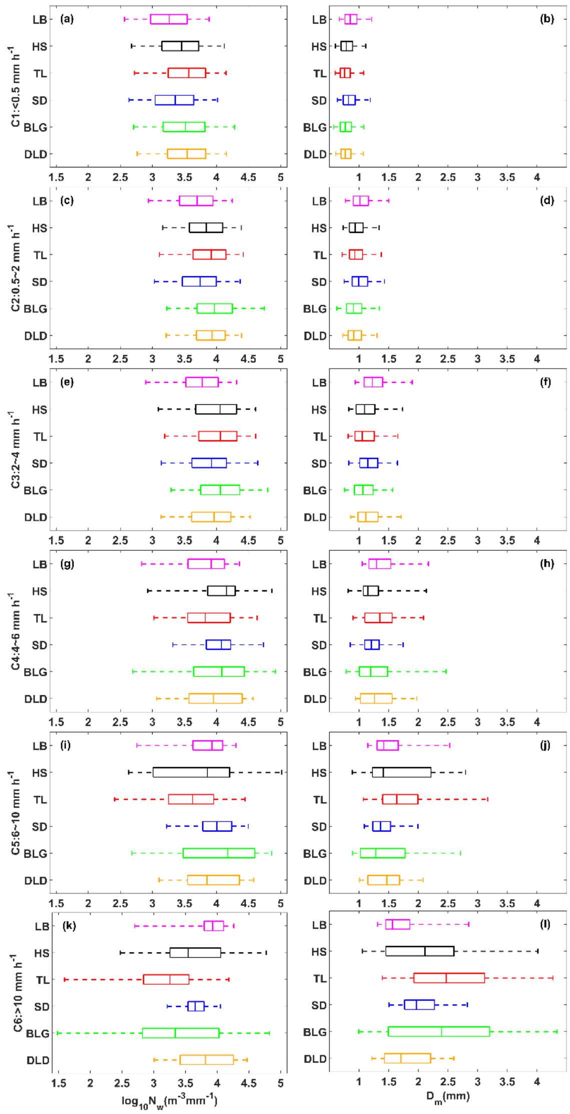

Fig.5 Variation of normalized intercept parameter $log_{10}N_w$ (a) and the mass-weighted mean diameter D_m (b) for different rain rate classes at 6 sites. The three lines in box are 25th, 50th and 75th percentiles from left to right, respectively. The whiskers on the left end and right end are 5th and 95th percentiles, respectively. The colors represent 6 sites same as other figures.

Figure 6 displays the contribution of different rain rate classes to the total rainfall at different sites. It is clear that C2 contributes the most to the total rainfall of all sites, followed by C3, and the sum of two classes of contribution could reach 60% to the total rainfall. Compared with the districts on the inside and southern slopes, C2 and C3

https://doi.org/10.5194/hess-2022-66
Preprint. Discussion started: 23 February 2022

contribute slightly less to LB and SD sites (i.e. the northern slopes), while C5 and C6 contribute relatively more to LB and SD sites, indicating that there is a greater probability of heavy precipitation events on the northern slopes. The DSD parameters in Table 3 provide a more detailed representation of the rainfall differences between the three geographic locations of the Qilian Mountains, namely the inside, southern slopes and northern slopes. Meanwhile, it also reflects the characteristics of rainfall on the eastern and middle sections, such as the eastern section has larger Z and D_m and smaller $\log_{10}N_w$ and $\log_{10}N_t$ compared to the middle section. It is possible that there is a certain spatial connection between precipitation at the sites, which is related to the factors like the source of precipitation vapor, weather system and so on.

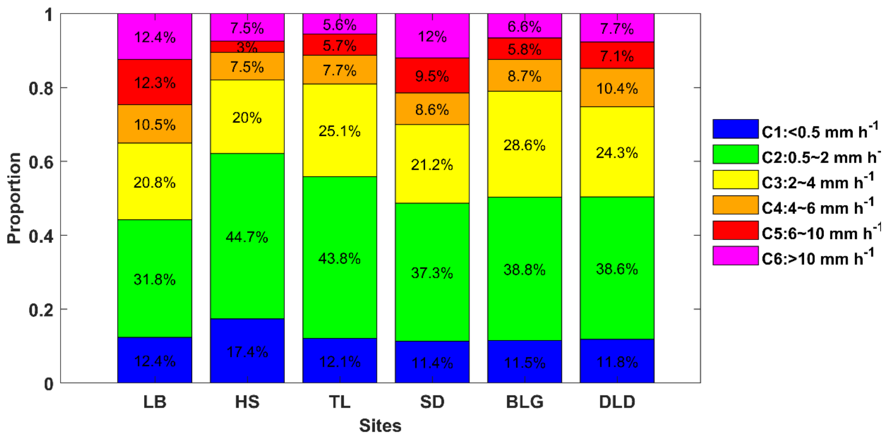

Fig.6 Proportion of rainfall with different rain rate classes to rain amount at 6 sites.

3.4 DSD properties for different rain types

Previous studies on DSD have shown that there are significant differences in the DSD of convective and stratiform rainfall in the same climatic region, which has a great impact on the parameterization of NWP and remote sensing observations (Bringi et al., 2003; Penide et al., 2013). Due to the different physical mechanisms of convective and stratiform rainfall, it can be allowed to discuss the differences of microphysical structures for rainfall types through their DSD. In some studies, there have been many classification methods for rainfall types, like Testud et al. (2001) used rain rate; Chen et al. (2013) combined rain rate and its standard deviation (SD); and Das et al. (2018) were based on rain rate and radar reflectivity factor. The method from Chen et al. (2013) was always used to establish samples of convective and stratiform rainfall, in which the studies' area were concentrated in semi-humid or humid regions with relatively high rain rate and rainfall. However, Qilian Mountains are located in the semi-arid regions of China and far from the sea, which the average rainfall rain and rainfall are quite different from the semi-humid regions. The paper therefore proposes a new classification method for precipitation applicable to the arid and semi-arid regions of northwest China based on the classification ideas of Chen and Saurabh.

Firstly, the sequences of DSD with continuous 1-min samples more than 10

https://doi.org/10.5194/hess-2022-66
Preprint. Discussion started: 23 February 2022

minutes are determined, and Rt is defined to denote the rain rate at time t. The first case: the R of samples from R_{t-5} to R_{t+5} are all less than 5mmh^{-1} and their standard deviation (SD) is less than 1.5 mmh^{-1}; the second case: the R of samples from R_{t-5} to R_{t+5} are greater than or equal to 5 mmh^{-1} with more than 9 samples and their SD is greater than 1.5 mmh^{-1}; the third case: same as the second case but their SD is less 1.5 mmh^{-1}. Secondly, samples satisfying Z<20 and W<0.08 in the second case are removed (Thurai et al., 2016; Das et al., 2018). And then, samples with R_t great than or equal to 5 mmh^{-1} in the second case are regarded as convective rainfall and samples with R_t less than 5 mmh^{-1} in the second case are regarded as transition rainfall (the rainfall stage in which convective precipitation develops and declines). Samples in the first case are regarded as stratiform rainfall. Through experiments, the third case does not exist.

The $\log_{10}N_w$ and D_m of different rainfall types are different, which make as the main research objects. Figure 7 shows the variation of $\log_{10}N_w$ with the D_m at different sites. The blue, red, and yellow scattered points represent stratiform, convective and transition rainfall, respectively. Obviously, there are fairly clear boundaries between the scatter points for different precipitation type events and the same dividing line can be used to distinguish different rainfall types at different sites. The black solid lines were drawn based on visual examination of the data with a slope of approximately -1.60 and intercept of 6.008 to represent the split between stratiform, transition and convective rainfall in all subplots. The black dashed line can distinguish transition rainfall (transition and stratiform rainfall have overlap area) with a slope of approximately -3.338 and intercept of 6.847. Note that the dividing line between stratiform and convective rainfall has the same slope obtained by Bringi et al. (2003) (solid green line with a slope of -1.6 and intercept of 6.3) who fitted the composite results based on disdrometer data and from radar retrievals covering many climate conditions from near equator to plateau. The $\log_{10}N_w$ and D_m from the figures to stratiform, convective and transition rainfall are respectively concentrated in 3.1-3.9 m^{-3}mm^{-1}, 0.75-1.1 mm; 3.8-4.2 m^{-3}mm^{-1}, 1.4-1.6 mm; 3.6-4.0 m^{-3}mm^{-1}, 1.05-1.2 mm. Compared to the maritime-like cluster and continental-like cluster of convective rainfall proposed by Bringi et al. (2003), the convective events in Qilian Mountains are more consistent with the continental-like cluster (the gray rectangle with smaller $\log_{10}N_w$ and larger D_m in Figure 7). There are isolated convective events in the maritime-like cluster, but it is difficult to have more events from the trend between log10N_w and D_m. This is also consistent with features of geographical location in Qilian Mountains.

https://doi.org/10.5194/hess-2022-66
Preprint. Discussion started: 23 February 2022

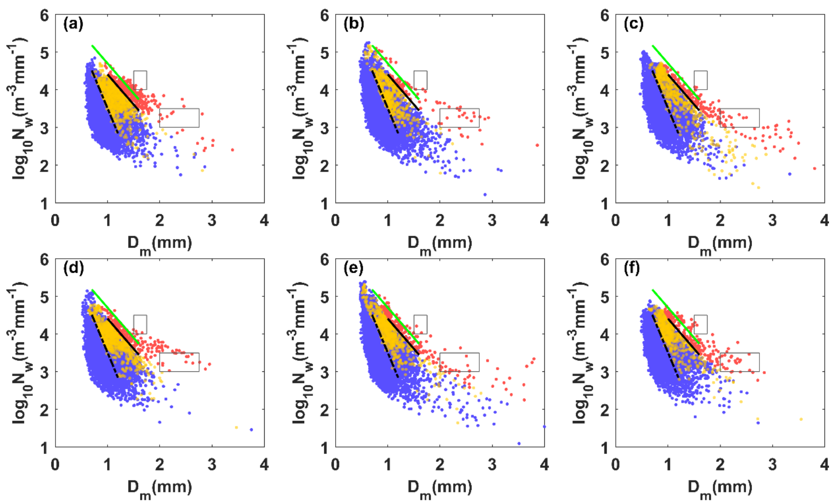

Fig.7 Scatter plot of $\log_{10}N_w$ versus Dm for different rain types at (a) LB, (b) HS, (c) TL, (d)SD, (e)BLG, (f)DLD. The stratiform cases, convective cases and transition cases are represented by blue, red and yellow circle dots, respectively. The black dashed lines are the $\log_{10}N_w$-D_m relationship for stratiform versus convective cases and stratiform versus transition case.

Figure 8 shows the mean DSDs for stratiform, convective and transition rainfall at six sites. The range of number concentrations and corresponding raindrop diameters for the three types are significantly different, matching the basic characteristics of DSD. The mean DSDs of stratiform rainfall differ slightly among sites; convective rainfall has big differences at sites; and transition rainfall appears more differences beginning at larger than 2.2 mm diameter, which are the expected results. Stratiform rainfall usually has a large horizontal extent and a homogeneous cloud distribution, which makes the DSD characteristics basically same under the influence of same cloud system in the mountainous areas. But convective rainfall is related to the local thermal and dynamical factors, which could lead to differences in the DSD at different sites adding the complex topography and diverse underlying in mountainous areas. For example, in convective rainfall, there is a significant increase in the number concentration of raindrops larger than 2.2 mm diameter at BLG, HS and TL, indicating that these districts are conducive to the development of convective precipitation. And the number concentration of small raindrops in BLG and HS is higher than that in TL (the southern slope), which may be due to the higher altitude of the inside sites reducing the falling distance of raindrops after exiting the cloud and decreasing the impact of collision on the raindrop evolution. In other words, even in the same rainfall type, the microphysical process of rainfall at different sites is still different, depending on the topography and position of the observation point relative to the cloud base.

https://doi.org/10.5194/hess-2022-66
Preprint. Discussion started: 23 February 2022

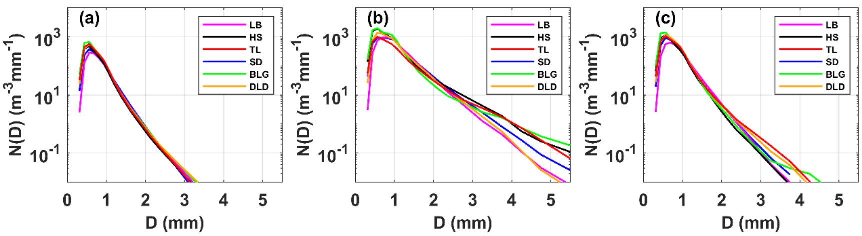

Fig.8 Distribution of mean measured DSD for (a) stratiform rainfall, (b) convective rainfall and (c) transition rainfall at 6 sites.

Figure 9 is the box-whisker plots of $log_{10}N_w$ and D_m for different rain types. The $log_{10}N_w$ and D_m of stratiform rainfall are smaller than that of convective rainfall but larger than that of transition rainfall. Sites with a large $log_{10}N_w$ value range have a larger values range for D_m; and sites with a large median for $log_{10}N_w$ have a smaller median for D_m, especially at HS and BLG sites in convective rainfall. Based on the mean value of six sites in Table 4, the DSD characteristic in Qilian Mountains consists of a larger N_w and a smaller D_m due to melting of tiny, compact graupel, and rimed ice particles (relative to large, low-density snowflakes). Compared with transition rainfall, the D_m of convective rainfall is obviously larger, indicating that the increase in rain rate in this area is mainly due to the growth in raindrop size. Moreover, the northern slopes should consider the increase of number concentration, because the $log_{10}N_w$ of convective rainfall also have increased. Note that the number of convective samples on the northern slope is higher than that of other sites, which correspond to the speculation in the contribution of different rain rate classes. On average of stratiform rainfall, the dispersion degree of $log_{10}N_w$ and D_m in different sites is 8.3% and 10.0%, respectively; and convective rainfall is 10.4%、23.4%, respectively. The standard deviations of DSD parameters at HS and BLG sites are relatively large.

Table 4 Statistical of several integral DSD parameters for six sites with stratiform rainfall, convective rainfall and transition rainfall

Type	Sites	Sample	$Log_{10}N_w$ ($m^{-3}mm^{-1}$)		Dm (mm)		μ		$Log_{10}N_t$ (m^{-3})		R (mmh^{-1})		Z dBZ	
			ME	SD	ME	SD	ME	SD	ME	SD	ME	SD	ME	SD
S	LB	7123	3.42	0.42	0.96	0.21	11.48	7.98	1.98	0.38	0.54	0.60	16.93	5.93
	HS	12694	3.60	0.44	0.88	0.21	11.24	7.89	2.14	0.40	0.54	0.58	16.17	6.06
	TL	10091	3.71	0.43	0.87	0.20	11.90	8.01	2.23	0.39	0.65	0.67	16.85	6.15
	SD	7175	3.51	0.44	0.95	0.22	11.15	8.03	2.07	0.39	0.62	0.64	17.36	6.10
	BLG	12467	3.72	0.49	0.88	0.23	12.24	8.50	2.25	0.44	0.70	0.74	17.11	6.33
	DLD	9685	3.70	0.42	0.88	0.21	11.91	7.91	2.23	0.38	0.67	0.69	17.18	6.13
C	LB	292	3.91	0.35	1.49	0.35	6.50	3.30	2.81	0.23	9.28	5.56	35.88	3.59
	HS	100	3.85	0.67	1.71	0.84	6.33	4.33	2.95	0.30	12.55	13.75	37.32	6.64
	TL	159	3.54	0.59	1.87	0.74	5.21	4.97	2.72	0.30	9.48	6.91	37.96	5.21
	SD	219	3.91	0.37	1.54	0.47	6.61	4.68	2.85	0.19	10.75	7.68	36.24	5.02

	BLG	198	3.91	0.74	1.64	0.97	8.00	7.37	3.00	0.27	10.57	15.49	36.29	6.75
	DLD	203	3.94	0.48	1.50	0.43	6.96	5.24	2.87	0.27	9.41	6.04	35.89	4.27
T	LB	787	3.76	0.39	1.15	0.21	8.37	4.35	2.47	0.31	2.16	1.25	26.42	3.89
	HS	541	3.89	0.49	1.05	0.29	8.98	6.74	2.59	0.33	1.81	1.15	24.79	3.89
	TL	465	3.77	0.70	1.22	0.49	8.81	6.91	2.56	0.44	2.30	1.21	27.10	4.39
	SD	819	3.87	0.41	1.12	0.26	8.23	5.46	2.59	0.28	2.28	1.18	26.59	4.04
	BLG	665	4.04	0.51	1.04	0.31	10.33	7.31	2.72	0.33	2.19	1.13	25.66	4.44
	DLD	503	3.95	0.46	1.10	0.30	8.69	6.16	2.67	0.31	2.35	1.17	26.60	4.20

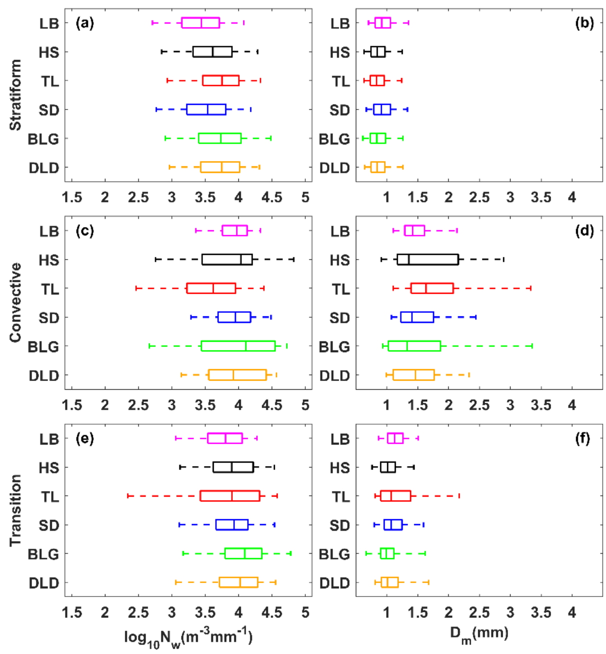

Fig.9 Same as Fig. 5 but for different rain types at 6 sites.

3.5 Implications for radar rainfall estimation with DSD

The sixth moment of raindrop diameter is proportional to the radar reflectivity factor and the 3.76 moment is approximately rain rate (they can be calculated by Equations 4 and 5). Generally, the theoretical basis of the QPE for single polarization radar (ground based or space based) is the power relationship between radar reflectivity and rainfall rate ($Z=AR^b$). This makes the coefficients A and exponents b of the power relationship heavily dependent on the variation of the DSD. Therefore, it is necessary to obtain the A and b of different sites according to different rainfall types.

Figure 10 shows the Z-R scatter plots for different sites and the fitted power-law relationships for different rainfall types. The blue and red scatters represent stratiform and convective rainfall, respectively. The purple, red and black solid lines indicate Z-R relationships for stratiform, convective and total rainfall, respectively. It shows that Z-R scatters for HS and BLG are relatively scattered around 5mmh-1 rain rate. Besides, the Z-R relationship of total rainfall underestimates stratiform rainfall at low R values

https://doi.org/10.5194/hess-2022-66
Preprint. Discussion started: 23 February 2022

and underestimates convective rainfall at high R values. On the average of Z-R relationship using a least-squares method, the dispersion degree of A and b in different sites is 42.5% and 10.7%, respectively, which reveal the large differences in mountains.

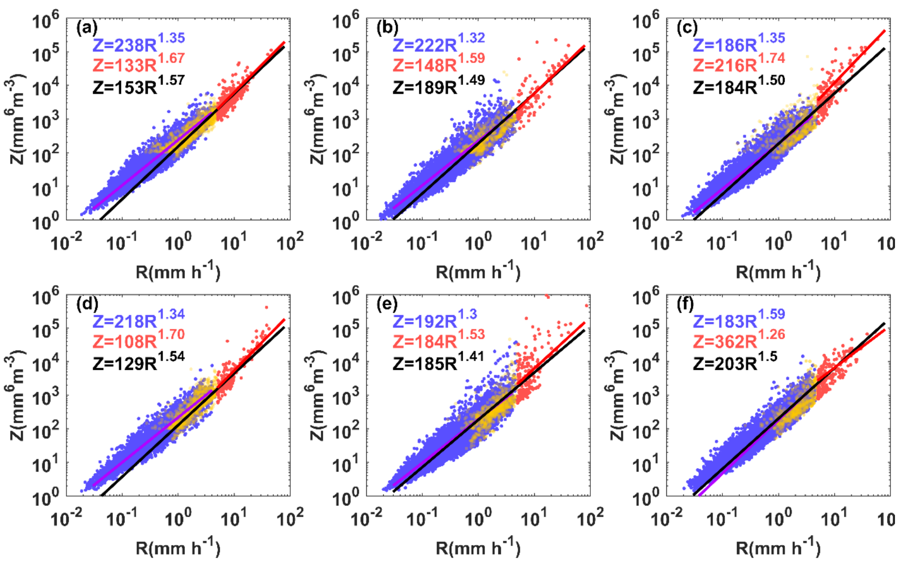

Fig.10 Scatter plot of Z (mm^6m^{-3}) versus R (mmh-1) for three rain types at (a) LB, (b) HS, (c) TL, (d)SD, (e)BLG, (f)DLD. The blue, red and yellow circle dots, respectively, stand for stratiform, convective and transition cases. The purple, red and black lines denote the Z-R relation. The blue, red and black formula denote stratiform, convective and total Z-R relationships.

In order to compare the six sites Z-R relationship with some standard Z-R relationships, $Z=300R^{1.4}$ for convective rainfall commonly used on radar and $Z=200R^{1.6}$ (i.e. M48) for stratiform rainfall commonly used on midlatitude areas are provided in figure 11. Overall, convective rainfall has smaller values of A and larger values of b than that of stratiform rainfall (excluding DLD). The A values of convective rainfall are smaller than the commonly used Z-R relationship with large differences, but the b values are greater. The distribution of A and b for stratiform rainfall is relatively concentrated with A and b ranging from 186-238 and 1.3-1.35, respectively. The A values of SR are close to the M48, and the b values are close to and smaller than the Z-R of global SR. The DLD station has a similar Z-R in stratiform rainfall with M48, while its convective rainfall is different from other sites with a larger A value (twice as large as other sites) and smaller b value. In addition, it can make it clear that the A value of stratiform rainfall increases from the southern slopes to northern slopes, while the convective rainfall is opposite. And the Z-R relationships of the same side are more consistent, such as both on inside or the northern slopes, which have geographic characteristics.

https://doi.org/10.5194/hess-2022-66
Preprint. Discussion started: 23 February 2022

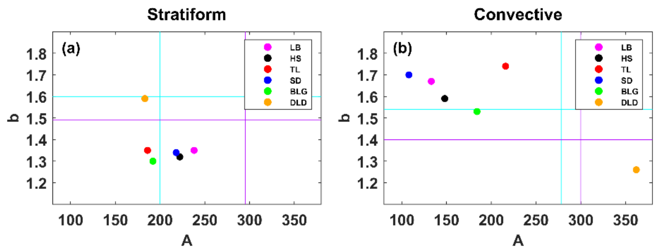

Fig.11 A and b values of the Z-R relationship for (a) stratiform rainfall and (b) convective rainfall at 6 sites. The purple lines in Fig. 12a and 12b correspond to the global Z-R model ($Z = 295R^{1.49}$ for continental stratiform rainfall and $Z = 278R^{1.54}$ for convective rainfall, respectively) (Ghada et al., 2018). The cyan line in Fig. 12a represents midlatitude stratiform rainfall Z-R model ($Z = 200R^{1.60}$, Marshall, 1948); the cyan line in Fig. 12b represents the convective rainfall Z-R model ($Z = 300R^{1.40}$) applied to the operational weather radar (Fulton et al., 1998).

4 Discussion

The paper analyses the statistical characteristics of DSD at different sites in the Qilian Mountains during the rainy season, which not only contain rainfall classes and rainfall types but more importantly reflect the differences between different sites. The results from different aspects can be mutually confirmed and have a good representation of the spatial distribution, making as a great factual basis for the discussion of the microphysical structure for precipitation. For example, with the rain rate class rising, the number concentration of all size bins is increased and the width of DSDs become wider, which as a feature are manifested in rain types that convective rainfall has a larger rain rate. In terms of spatiality, the characteristics of precipitation on the inside and southern slope are closer, whether the overall DSD or the DSD parameter distribution. But there are some obvious variabilities in the inside mountains for DSD parameters due to the influences of its local dynamics and thermal. On the other hand, these characteristics also exhibit some differences between the middle and eastern sections in Qilian Mountains, especially in the discussion of DSD parameters for rainfall classes and rainfall types (shown as Figures 5 and 9). This spatial variation in DSD suggests that microphysical processes in DSD are influenced by complex topography (altitude, mountain alignment) and potentially related to the source of water vapor, development of precipitation process and anthropogenic factors.

Compared to the precious studies that are focused on eastern, southern and northern China as well Tibetan Plateau, the Qilian Mountains have its own unique DSD characteristics and Z-R relationship during the rainy season, which include the smaller raindrop diameter with higher number concentration. Moreover, the division of rain rate classes in Qilian Mountains more adequately reflects the DSD characteristics at each class, unlike using the classification method of other sites with larger rain rates. Above all, it is Qilian Mountains that the proposed classification of stratiform and convective rainfall is applicable to, which is located on the arid and semi-arid regions.

As aforementioned, the characteristics of DSD mainly describe on the diameters

https://doi.org/10.5194/hess-2022-66
Preprint. Discussion started: 23 February 2022

larger than 0.2 mm, which are limited by the observation instruments that cannot detect the small drops on diameter less than 0.2 mm. So, it is not a complete DSD and underestimates the number concentration of small drops on diameter less than 0.5 mm. Recent studies have been devoted to improving DSD observations in order to overcome the limitations of disdrometer. A study by Thurai et al. (2017) have obtained a more complete DSD by splicing the 2DVD and MPS (Meteorological Particle Spectrometer) to observe DSD and developed a technology to reconstruct the drizzle mode DSD (Raupach et al., 2019), which has a good presentation to the DSD of small raindrops and more important applications.

5 Summary and conclusion

Based on the six-months DSD data observed in the southern slopes, northern slopes and inside of Qilian Mountains, the characteristics and their differences of DSD are studied, and Z-R relationships of six districts are discussed. The main conclusions are as follows.

For small raindrops, the number concentrations on the inside and southern slopes districts are greater than that on the northern slopes; for midsize raindrops, the number concentrations decrease sequentially on the northern slopes, southern slopes and inside districts; for large raindrops, the number concentrations on the inside districts are larger. In addition, the number concentrations of raindrops in the middle section of the mountainous area is slightly greater than that in the eastern section.

1. For all rainfall events, the number concentration of small and large raindrops on the inside and southern slopes are greater than that on the northern slope, while midsize raindrops are less. The DSD of inside mountains has a great variability, which is quite different from the northern slope.
2. The DSDs are divided into six categories based on rainfall rate: C1, $R<0.5$; C2, $0.5\leqslant R<2$; C3, $2\leqslant R<4$; C4, $4\leqslant R<6$; C5, $6\leqslant R<10$; C6, >10 mm h-1. As the rain rate increases, the median of D_m for each station is gradually larger and the median of N_w rises on C1-C3 and then decreases on C4-C6, as well the differences of number concentration on each drop size increases. Especially in the inside mountains. The most contribution to the total rainfall at different sites is C2 class and C3 class next, with the sum of contribution reaching 60%. Besides, the C5 and C6 class have a relatively large contribution to the north slope with a greater probability of heavy precipitation events.
3. There is a rather clear boundary in the distribution of $\log_{10}N_w$ versus D_m between the rainfall types, which the split line between stratiform and convective rainfall has the same slope with the line given by Bringi et al. The dispersion degree of $\log_{10}N_w$ and D_m at sites are 8.3% and 10.0% for stratiform rainfall and 10.4% and 23.4% for convective rainfall, respectively. The standard deviations of DSD parameters on inside sites are larger, making it easier to increase the number concentration of large raindrops in convective rainfall.
4. The Z-R relationships of different sites in stratiform rainfall are similar and generally underestimated by the $Z=200R^{1.6}$ model used to the midlatitude stratiform rainfall; the Z-R relationships for convective precipitation vary greatly

https://doi.org/10.5194/hess-2022-66
Preprint. Discussion started: 23 February 2022

at different station, which are overestimated by $Z=300R^{1.4}$ at lower rain rates values and underestimated at higher rain rates values. The dispersion degree of coefficient A and exponent b in Z-R relationship for sites are 42.5% and 10.7%, respectively. Overall, the A value of stratiform rainfall increases from the southern slopes to northern slopes, while the convective rainfall is opposite. And the Z-R relationships of the ipsilateral sites are more consistent.

5. The analysis of DSD and DSD parameters can reflect the characteristics of the southern slope, northern slope and inside sites, as well as the differences between the eastern and middle sections of Qilian Mountains.

This study reveals the microphysical variability of precipitation in the complex topography of the arid and semi-arid regions of Northwest China, which can not only improve local numerical simulations, but also provides a basis for further understanding of the differences in DSD characteristics formed at mesoscale due to topographic factors and water vapor distribution, etc. It is important to note that this should be one of the fundamental studies for the future implementation of weather modification, which is of great significance to solving the shortage of water resources in the arid and semi-arid regions.

Data availability. Disdrometer data used in this study are available by contacting the authors.

Author contributions. WM conducted the detailed analysis; WZ provided financial support and conceived the idea; MK collated the observation data; all the authors contributed to the writing and revisions.

Competing interests. The authors declare that they have no conflict of interest.

Acknowledgments

The work was supported by Weather modification ability construction project of Northwest China under grant No. ZQC-R18208 and The Second Tibetan Plateau Comprehensive Scientific Expedition Grant No. 2019QZKK0104.

https://doi.org/10.5194/hess-2022-66
Preprint. Discussion started: 23 February 2022

Hydrology and Earth System Sciences
Open Access
Discussions

References

Adirosi, E., N. Roberto, M. Montopoli, E. Gorgucci, and L. Baldini, 2018: Influence of disdrometer type on weather radar algorithms from measured DSD: Application to Italian climatology. Atmosphere, 9, 360.

Angulo-Martínez, M., and A. Barros, 2015: Measurement uncertainty in rainfall kinetic energy and intensity relationships for soil erosion studies: An evaluation using PARSIVEL disdrometers in the Southern Appalachian Mountains. Geomorphology, 228, 28-40.

Atlas, D., R. Srivastava, and R. S. Sekhon, 1973: Doppler radar characteristics of precipitation at vertical incidence. Reviews of Geophysics, 11, 1-35.

Bringi, V., V. Chandrasekar, J. Hubbert, E. Gorgucci, W. Randeu, and M. Schoenhuber, 2003: Raindrop size distribution in different climatic regimes from disdrometer and dual-polarized radar analysis. Journal of the atmospheric sciences, 60, 354-365.

Campos, E., I. Zawadzki, M. Petitdidier, and W. Fernandez, 2006: Measurement of raindrop size distributions in tropical rain at Costa Rica. Journal of Hydrology, 328, 98-109.

Chen, B., J. Yang, and J. Pu, 2013: Statistical characteristics of raindrop size distribution in the Meiyu season observed in eastern China. Journal of the Meteorological Society of Japan. Ser. II, 91, 215-227.

Dolan, B., B. Fuchs, S. Rutledge, E. Barnes, and E. Thompson, 2018: Primary modes of global drop size distributions. Journal of the Atmospheric Sciences, 75, 1453-1476.

Das, S., and A. Maitra, 2018: Characterization of tropical precipitation using drop size distribution and rain rate-radar reflectivity relation. Theoretical and applied climatology, 132, 275-286.

Fu, Z., and Coauthors, 2020: Statistical characteristics of raindrop size distributions and parameters in Central China during the Meiyu seasons. Journal of Geophysical Research: Atmospheres, 125, e2019JD031954.

Fulton, R. A., J. P. Breidenbach, D.-J. Seo, D. A. Miller, and T. O'Bannon, 1998: The WSR-88D rainfall algorithm. Weather and forecasting, 13, 377-395.

Geoffroy, O., A. Siebesma, and F. Burnet, 2014: Characteristics of the raindrop distributions in RICO shallow cumulus. Atmospheric Chemistry and Physics, 14, 10897-10909.

Ghada, W., A. Buras, M. Lüpke, C. Schunk, and A. Menzel, 2018: Rain microstructure parameters vary with large-scale weather conditions in Lausanne, Switzerland. Remote Sensing, 10, 811.

Giannetti, F., and Coauthors, 2017: Real-time rain rate evaluation via satellite downlink signal attenuation measurement. Sensors, 17, 1864.

Gou, X., F. Chen, M. Yang, J. Li, J. Peng, and L. Jin, 2005: Climatic response of thick leaf spruce (Picea crassifolia) tree-ring width at different elevations over Qilian Mountains, northwestern China. Journal of Arid Environments, 61, 513-524.

https://doi.org/10.5194/hess-2022-66
Preprint. Discussion started: 23 February 2022

Jash, D., E. Resmi, C. Unnikrishnan, R. Sumesh, T. Sreekanth, N. Sukumar, and K. Ramachandran, 2019: Variation in rain drop size distribution and rain integral parameters during southwest monsoon over a tropical station: An inter-comparison of disdrometer and Micro Rain Radar. Atmospheric Research, 217, 24-36.

Kruger, A., and W. F. Krajewski, 2002: Two-dimensional video disdrometer: A description. Journal of Atmospheric and Oceanic Technology, 19, 602-617.

Le Loh, J., D.-I. Lee, and C.-H. You, 2019: Inter-comparison of DSDs between Jincheon and Miryang at South Korea. Atmospheric Research, 227, 52-65.

Li, Z., and Coauthors, 2019: Climate background, relative rate, and runoff effect of multiphase water transformation in Qilian Mountains, the third pole region. Science of The Total Environment, 663, 315-328.

Lim, Y. S., J. K. Kim, J. W. Kim, B. I. Park, and M. S. Kim, 2015: Analysis of the relationship between the kinetic energy and intensity of rainfall in Daejeon, Korea. Quaternary International, 384, 107-117.

Ma, L., L. Zhao, D. Yang, Y. Xiao, L. Zhang, and Y. Qiao, 2019a: Analysis of Raindrop Size Distribution Characteristics in Permafrost Regions of the Qinghai–Tibet Plateau Based on New Quality Control Scheme. Water, 11, 2265.

Ma, Y., G. Ni, C. V. Chandra, F. Tian, and H. Chen, 2019b: Statistical characteristics of raindrop size distribution during rainy seasons in the Beijing urban area and implications for radar rainfall estimation. Hydrology and Earth System Sciences, 23, 4153-4170.

Marshall, J. S., 1948: The distribution of raindrops with size. J. meteor., 5, 165-166.

McFarquhar, G. M., T.-L. Hsieh, M. Freer, J. Mascio, and B. F. Jewett, 2015: The characterization of ice hydrometeor gamma size distributions as volumes in N0–λ–μ phase space: Implications for microphysical process modeling. Journal of Atmospheric Sciences, 72, 892-909.

Narayana Rao, T., N. Kirankumar, B. Radhakrishna, and D. Narayana Rao, 2006: On the variability of the shape-slope parameter relations of the gamma raindrop size distribution model. Geophysical research letters, 33.

Protat, A., and Coauthors, 2019: The latitudinal variability of oceanic rainfall properties and its implication for satellite retrievals: 1. Drop size distribution properties. Journal of Geophysical Research: Atmospheres, 124, 13291-13311.

Pu, K., X. Liu, Y. Wu, S. Hu, L. Liu, and T. Gao, 2020: A comparison study of raindrop size distribution among five sites at the urban scale during the East Asian rainy season. Journal of Hydrology, 590, 125500, https://doi.org/10.1016/j.jhydrol.2020.125500.

Penide, G., A. Protat, V. V. Kumar, and P. T. May, 2013: Comparison of two convective/stratiform precipitation classification techniques: Radar reflectivity texture versus drop size distribution–based approach. Journal of Atmospheric and Oceanic Technology, 30, 2788-2797.

Qin, Y., H. Lei, D. Yang, B. Gao, Y. Wang, Z. Cong, and W. Fan, 2016: Long-term change in the depth of seasonally frozen ground and its ecohydrological impacts

https://doi.org/10.5194/hess-2022-66
Preprint. Discussion started: 23 February 2022

in the Qilian Mountains, northeastern Tibetan Plateau. Journal of Hydrology, 542, 204-221.

Rincon, R. F., and R. H. Lang, 2002: Microwave link dual-wavelength measurements of path-average attenuation for the estimation of drop size distributions and rainfall. IEEE Transactions on geoscience and remote sensing, 40, 760-770.

Raupach, T. H., M. Thurai, V. Bringi, and A. Berne, 2019: Reconstructing the drizzle mode of the raindrop size distribution using double-moment normalization. Journal of Applied Meteorology and Climatology, 58, 145-164.

Seela, B. K., J. Janapati, P. L. Lin, K. K. Reddy, R. Shirooka, and P. K. Wang, 2017: A comparison study of summer season raindrop size distribution between Palau and Taiwan, two islands in western Pacific. Journal of Geophysical Research: Atmospheres, 122, 11,787-711,805.

Smith, J. A., E. Hui, M. Steiner, M. L. Baeck, W. F. Krajewski, and A. A. Ntelekos, 2009: Variability of rainfall rate and raindrop size distributions in heavy rain. Water Resources Research, 45.

Thurai, M., P. Gatlin, and V. Bringi, 2016: Separating stratiform and convective rain types based on the drop size distribution characteristics using 2D video disdrometer data. Atmospheric Research, 169, 416-423.

Thurai, M., P. Gatlin, V. Bringi, W. Petersen, P. Kennedy, B. Notaroš, and L. Carey, 2017: Toward completing the raindrop size spectrum: Case studies involving 2D-video disdrometer, droplet spectrometer, and polarimetric radar measurements. Journal of Applied Meteorology and Climatology, 56, 877-896.

Testud, J., S. Oury, R. A. Black, P. Amayenc, and X. Dou, 2001: The concept of "normalized" distribution to describe raindrop spectra: A tool for cloud physics and cloud remote sensing. Journal of Applied Meteorology, 40, 1118-1140.

Tian, H., T. Yang, and Q. Liu, 2014: Climate change and glacier area shrinkage in the Qilian mountains, China, from 1956 to 2010. Annals of Glaciology, 55, 187-197.

Wainwright, C. E., D. T. Dawson, M. Xue, and G. Zhang, 2014: Diagnosing the intercept parameters of the exponential drop size distributions in a single-moment microphysics scheme and impact on supercell storm simulations. Journal of Applied Meteorology and Climatology, 53, 2072-2090.

Wang, Y., J. Zheng, Z. Cheng, and B. Wang, 2020: Characteristics of Raindrop Size Distribution on the Eastern Slope of the Tibetan Plateau in Summer. Atmosphere, 11, 562.

Wu, Y., and L. Liu, 2017: Statistical characteristics of raindrop size distribution in the Tibetan Plateau and southern China. Advances in Atmospheric Sciences, 34, 727-736.

Yang, L., J. Smith, M. L. Baeck, B. Smith, F. Tian, and D. Niyogi, 2016: Structure and evolution of flash flood producing storms in a small urban watershed. Journal of Geophysical Research: Atmospheres, 121, 3139-3152.

Zhang, A., and Coauthors, 2019: Statistical characteristics of raindrop size distribution in the monsoon season observed in southern China. Remote Sensing, 11, 432.

https://doi.org/10.5194/hess-2022-66
Preprint. Discussion started: 23 February 2022

Zhao, P., and Coauthors, 2019: The Tibetan Plateau surface-atmosphere coupling system and its weather and climate effects: The Third Tibetan Plateau Atmospheric Science Experiment. Journal of Meteorological Research, 33, 375-399.

Zeng, Y., and Coauthors, 2021: Statistical Characteristics of Raindrop Size Distribution during Rainy Seasons in Northwest China. Advances in Meteorology, 2021.